Probing the Differences between Rat Liver Outer Mitochondrial Membrane Cytochrome b_5 and Microsomal Cytochromes b_5[†]

Adriana Altuve,[‡] Svetlana Silchenko,[§] Kyung-Hoon Lee,[§] Krzysztof Kuczera,[§] Simon Terzyan,[||] Xuejun Zhang,[||] David R. Benson,*[,§] and Mario Rivera*[,‡]

Department of Chemistry, Oklahoma State University, Stillwater, Oklahoma 74078-3071, Department of Chemistry, University of Kansas, Lawrence, Kansas 66045, and Crystallography Program, Oklahoma Medical Research Foundation, 825 NE 13th Street, Oklahoma City, Oklahoma 73104

Received March 29, 2001; Revised Manuscript Received May 28, 2001

ABSTRACT: Two distinct forms of cytochrome b_5 exist in the rat hepatocyte. One is associated with the membrane of the endoplasmic reticulum (microsomal, or Mc, cyt b_5) while the other is associated with the outer membrane of liver mitochondria (OM cyt b_5). Rat OM cyt b_5, the only OM cyt b_5 identified so far, has a significantly more negative reduction potential and is substantially more stable toward chemical and thermal denaturation than Mc cytochromes b_5. In addition, hemin is kinetically trapped in rat OM cyt b_5 but not in the Mc proteins. As a result, no transfer of hemin from rat OM cyt b_5 to apomyoglobin is observed at pH values as low as 5.2, nor can the thermodyamically favored ratio of hemin orientational isomers be achieved under physiologically relevant conditions. These differences are striking given the similarity of the respective protein folds. A combined theoretical and experimental study has been conducted in order to probe the structural basis behind the remarkably different properties of rat OM and Mc cytochromes b_5. Molecular dynamics (MD) simulations starting from the crystal structure of bovine Mc cyt b_5 revealed a conformational change that exposes several internal residues to the aqueous environment. The new conformation is equivalent to the "cleft-opened" intermediate observed in a previously reported MD simulation of bovine Mc cyt b_5 [Storch, E. M., and Daggett, V. (1995) *Biochemistry 34*, 9682−9693]. The rat OM protein does not adopt a comparable conformation in MD simulations, thus restricting access of water to the protein interior. Subsequent comparisons of the protein sequences and structures suggested that an extended hydrophobic network encompassing the side chains of Ala-18, Ile-32, Leu-36, and Leu-47 might contribute to the inability of rat OM cyt b_5 to adopt the cleft-opened conformation and, hence, stabilize its fold relative to the Mc isoforms. A corresponding network is not present in bovine Mc cyt b_5 because positions 18, 32, and 47, are occupied by Ser, Leu, and Arg, respectively. To probe the roles played by Ala-18, Ile-32, and Leu-47 in endowing rat OM cyt b_5 with its unusual structural properties, we have replaced them with the corresponding residues in bovine Mc cyt b_5. Hence, the I32L (single), A18S/L47R (double), and A18S/L47R/I32L (triple) mutants of rat OM cyt b_5 were prepared. The stability of these proteins was found to decrease in the following order: WT rat OM > rat OM I32L > rat OM A18S/L47R > rat OM A18S/L47R/I32L > bovine Mc cyt b_5. The decrease in stability of the rat OM protein correlates with the extent to which the hydrophobic cluster involving the side chains of residues 18, 32, 36, and 47 has been disrupted. Complete disruption of the hydrophobic network in the triple mutant is confirmed in a 2.0 Å resolution crystal structure of the protein. Disruption of the hydrophobic network also facilitates hemin loss at pH 5.2 for the double and triple mutants, with the less stable triple mutant exhibiting the greater rate of hemin transfer to apomyoglobin. Finally, ^{1}H NMR spectroscopy and side-by-side comparisons of the crystal structures of bovine Mc, rat OM, and rat OM A18S/L47R/I32L cyt b_5 allowed us to conclude that the nature of residue 32 plays a key role in controlling the relative stability of hemin orientational isomers A and B in rat OM cyt b_5. A similar analysis led to the conclusion that Leu-70 and Ser-71 play a pivotal role in stabilizing isomer A relative to isomer B in Mc cytochromes b_5.

Two distinct forms of cytochrome b_5 have been shown to exist in the rat hepatocyte. One is associated with the membrane of the endoplasmic reticulum (microsomal, or Mc,[1] cytochrome b_5) while the other is associated with the outer membrane of liver mitochondria (OM cytochrome b_5). Both proteins are anchored to their respective membranes via a stretch of hydrophobic amino acids near the C-terminus. Mc cytochromes b_5 have been identified in mammals, insects,

[†] This work was supported by grants from the National Institutes of Health (GM 50503 to M.R. and GM 52431 to D.R.B.), OCAST (HR00-043 to M.R.), and the Petroleum Research Fund (33126-AC4 to K.K.).

* Correspondence should be addressed to these authors. M.R.: e-mail, rivera@okstate.edu. D.R.B.: e-mail, drb@ku.edu.

[‡] Oklahoma State University.

[§] University of Kansas.

[||] Oklahoma Medical Research Foundation.

[1] Abbreviations: Mc, microsomal; OM, outer membrane of mitochondria; cyt, cytochrome; MD, molecular dynamics; Mb, myoglobin; PEG, poly(ethylene glycol); GdmCl, guanidinium chloride.

10.1021/bi010636i CCC: $20.00
Published on Web 07/17/2001

```
                -16             -1 1          11          21          31
Bovine Mc         ----------MAEES SKAVKYYTLE EIQKHNNSKS TWLILHYKVY DLTKFLEEHP
Rabbit Mc         ----------MAAQS DKDVKYYTLE EIKKHNHSKS TWLILHHKVY DLTKFLEEHP
Porcine Mc        ----------MAEQS DKAVKYYTLE EIQKHNNSKS TWLILHHKVY DLTKFLEEHP
Mouse Mc          ----------MAGQS DKDVKYYTLE EIQKHKDSKS TWVILHHKVY DLTKFLEEHP
Human Mc          ----------MAEQS DEAVKYYTLE EIQKHNHSKS TWLILHHKVY DLTKFLEEHP
Rat Mc            ----------MAEQS DKDVKYYTLE EIQKHKDSKS TWVILHHKVY DLTKFLEEHP
Rat OM            MATPEASGSGRNGQGS DPAVTYYRLE EVAKRNTAEE TWMVIHGRVY DHTRFLSEHP

           41          51          61          71          81          91
Bovine Mc  GGEEVLREQA GGDATENFED VGHSTDAREL SKTFIIGELH PDDRSKITKP SESIITTIDS
Rabbit Mc  GGEEVLREQA GGDATENFED VGHSTDAREL SKTFIIGELH PDDRSKLSKP METLITTVDS
Porcine Mc GGEEVLREQA GGDATENFED VGHSTDAREL SKTFIIGELH PDDRSKIAKP SETLITTVES
Mouse Mc   GGEEVLREQA GGDATENFED VGHSTDAREL SKTYIIGELH PDDRSKIAKP SDTLITTVES
Human Mc   GGEEVLREQA GGDATENFED VGHSTDAREM SKTFIIGELH PDDRPKLNKP PETLITTIDS
Rat Mc     GGEEVLREQA GGDATENFED VGHSTDAREL SKTYIIGELH PDDRSKIAKP SETLITTVES
Rat OM     GGEEVLEEQA GADATESFED VGHSPDAREM LKQYYIGDVH PNDLK--PKD GDKDPSKNNS
```

FIGURE 1: Amino acid sequence alignments for heme-binding domains of mammalian Mc and OM cytochromes b_5 for which genes have been cloned. The sequences shown represent residues 1−105 and 1−114 of the full-length Mc and OM cytochromes, respectively (continued in Figure 2). The numbering scheme utilized, initially introduced by Mathews (*24*), is used to identify residues in the present work. Heme iron ligands His-39 and His-63 are shown in bold. Residues in rat OM cyt b_5 that were mutated as part of this work are highlighted against a black background.

```
           106         116         126       134
Bovine Mc    NPSWWTNWLI  PAISALFVAL  IYHLYTSEN
Rabbit Mc    NSSWWTNWVI  PAISALIVAL  MYRLYMADD
Porcine Mc   NSSWWTNWVI  PAISALVVSL  MYHFYTSEN
Mouse Mc     NSSWWTNWVI  PAISALAVAL  MYRLYMAED
Human Mc     SSSWWTNWVI  PAISAVAVAL  MYRLYMAED
Rat Mc       NSSWWTNWVI  PAISALVVAL  MYRLYMAED

           115         125         135           146
Rat OM       CQSSWAYWIV  PIVGAILIGF  LYRHFWADSK  SS
```

FIGURE 2: Continuation of the sequences shown in Figure 1, with residue numbers based on the actual protein sequence. The putative membrane-spanning regions are shown in bold.

plants, and a variety of other eukaryotes (*1*, *2*). In contrast, the only OM cyt b_5 that has been positively identified and studied to date originates from rat liver (*3*, *4*). In 1973, Fukushima and Sato reported that the heme-binding domain of rat liver OM cyt b_5, isolated from mitochrondria by treatment with trypsin, was immunologically distinct from the trypsin-cleaved heme-binding domain of rat liver Mc cyt b_5 (*3*). In 1980, Ito reported a method for obtaining the trypsin-cleaved heme-binding domain of rat liver OM cyt b_5 in high purity (*4*). Lederer and co-workers subsequently sequenced the heme-binding domain of trypsin-cleaved rat OM cyt b_5 and found it to be 58% homologous to the corresponding domain of rat liver Mc cyt b_5 (*5*). These early findings indicating the presence of two isoforms of cyt b_5 in the rat hepatocyte have been confirmed by reports demonstrating that rat liver Mc cyt b_5 and rat liver OM cyt b_5 are coded by different genes (*6*−*8*).

The amino acid sequences of several mammalian cytochromes b_5 are compared in Figures 1 and 2. Mc cytochromes b_5 and rat OM cyt b_5 possess an amino-terminal hydrophilic domain, a medial hydrophobic domain, and a carboxyl-terminal hydrophilic domain. The N-terminal domain (sequence shown in Figure 1) contains approximately 100 amino acid residues and binds protoheme IX (*9*). This portion of the protein extends into the cytosol where it participates in electron-transfer reactions (*10*−*13*). The medial hydrophobic domain, consisting of about 20 amino acids near the protein C-terminus (see Figure 2), is embedded in the lipid bilayer and anchors the protein to the appropriate membrane (*14*). The C-terminal domain of Mc cyt b_5, comprising about 7 residues, is exposed to the lumen of the ER (*15*, *16*). The corresponding domain of rat OM cyt b_5, containing about 10 residues, is most likely directed toward the intermembrane space of the mitochondrion.

It has been demonstrated that the carboxyl-terminal 10 amino acid residues of cyt b_5 (see Figure 2) possess the necessary information to determine whether the protein is localized to the ER (Mc cytochromes b_5) or to the outer mitochondrial membrane (OM cyt b_5) (*6*, *8*, *9*). For instance, when Lys-144 in rat OM cyt b_5 was replaced by Ala, and the K144A mutant was expressed in COS-7 cells, the mutant protein was localized to the ER membrane rather than the outer mitochondrial membrane. On the other hand, when Asp-134 in rat Mc cyt b_5 was replaced by Lys, the D134K mutant was localized mainly to the outer mitochondrial membrane (*8*). It was therefore concluded that localization of cyt b_5 to the outer mitochondrial membrane requires a positively charged residue near the C-terminus.

Genes for Mc cytochromes b_5 from several mammals have been cloned from cDNA libraries (*6*, *17*−*21*). All of these genes code for proteins containing 134 residues. A comparison of mammalian Mc cytochrome b_5 sequences using the program BlastP (*22*) (with bovine Mc cyt b_5 as the query) showed that the full-length proteins share 84−97% sequence identity and 93−98% sequence similarity. By comparison, full-length rat OM cyt b_5, at 146 amino acids (*8*), is longer than the Mc isoforms. Furthermore, a pairwise BlastP comparison of the full-length bovine Mc and rat OM cytochromes b_5 showed that they share only 49% sequence identity and 68% sequence similarity. The alignment generated by the algorithm begins with residue −1 for both proteins (refer to Figure 1) and ends at residue 134 for bovine Mc cyt b_5 and at residue 143 for rat OM cyt b_5 (see Figure 2). On the basis of the amino acid sequence reported by Lederer et al. (*5*), Rivera et al. (*23*) constructed a synthetic gene for expressing the water-soluble domain of rat OM cyt b_5. The recombinant protein consists of residues −5 to 87 according to the numbering scheme in Figure 1, initially used by Mathews for the structure of the lipase fragment of bovine Mc cyt b_5 (*24*). Subsequent X-ray and NMR structures deposited in the Protein Data Bank (PDB) maintained Mathew's original numbering scheme. For reasons of consistency, in our current and previous work with rat OM cyt b_5, we have also maintained this numbering scheme. As noted in a recent communication (*25*), the recombinant protein contains Asp at position −5 rather than Asn due to an error in the originally reported protein sequence. Comparison of UV/vis, EPR, and paramagnetic ^{1}H NMR data

suggested similar heme environments for the recombinant rat OM cyt b_5 and the Mc isoforms (*23*). The X-ray crystal structure (*26*) of the heme-binding domain of rat OM cyt b_5 confirmed that prediction, demonstrating that the recombinant protein adopts a fold identical in most respects to that characteristic of the Mc cytochromes b_5 (*27*). In fact, the rms difference between the crystal structure coordinates of the backbone atoms in rat OM and bovine Mc cyt b_5 (*27*) is 0.6 Å. The similarity of the two proteins is not only confined to the protein backbone but extends to the side chain rotamers; i.e., the side chain torsional angles of most residues differ by less than 60° (*26*).

Given the structural similarity between rat OM cyt b_5 and the Mc cytochromes b_5, it was striking to find that the reduction potential of rat OM cyt b_5 (−107 mV vs NHE) (*28*−*30*) is 100 mV more negative than the reduction potential of mammalian Mc cytochromes b_5 (0 ± 10 mV vs NHE) (*31*−*34*). More recently, we reported that oxidized rat OM cyt b_5 is also much more stable to thermal and chemical denaturation than oxidized Mc cytochromes b_5. Hemin release and reorientation are also dramatically slower in the mitochondrial isoform (*25*). The corresponding apoproteins have very similar stabilities, hence suggesting that stronger interactions between hemin (oxidized heme) and polypeptide in rat OM cyt b_5 contribute to its enhanced thermal and chemical stability. It is therefore interesting to ponder whether nature has tailored the biophysical properties of OM and Mc cytochrome b_5 so that each protein performs distinct roles in the cell. In this context it is illustrative to consider the only well-established function of rat OM cyt b_5, namely, its participation in the reduction of cytosolic semidehydroascorbate (ascorbate radical). To accomplish this function, electrons originating in NADH are transferred to NADH cyt b_5 reductase, which reduces OM cyt b_5 in the outer mitochondrial membrane. Reduced OM cyt b_5, in turn, transfers the electron to semidehydroascorbate reductase (*35*, *36*). Comparing the reduction potentials of rat OM cyt b_5 (−107 mV vs NHE) (*28*, *29*) and rat Mc cyt b_5 (−7 mV vs NHE) (*34*), it appears that only the mitochondrial isoform is likely to efficiently reduce semidehydroascorbate (E_0 = −10 mV vs NHE) (*37*).

The markedly different properties of rat OM cyt b_5 relative to the Mc isoforms are intriguing, considering that their crystal structures revealed only minor differences in overall fold (*26*). Consequently, this case represents an unparalleled opportunity to study how nature tuned the distinct properties of the OM and Mc cyt b_5 isoforms with minor variations in amino acid sequence and with subtle structural modifications. Herein we report the results of theoretical and experimental studies aimed at elucidating the factors responsible for the markedly higher stability and slower hemin release and reorientation in the rat OM protein relative to the Mc isoforms. Careful comparisons of the corresponding protein sequences and structures in the context of molecular dynamics (MD) simulations of rat OM and bovine Mc cyt b_5 suggested that an extended hydrophobic network involving the side chains of Ala-18, Ile-32, Leu-36, and Leu-47 in the rat OM isoform contributes to tight packing of a short surface loop consisting of residues 49−51. Much less extensive interactions occur among the side chains of Ser-18, Leu-32, Leu-36, and Arg-47 in bovine Mc cyt b_5. We hypothesized that this difference is responsible for opening of a large cleft on the surface of the Mc protein, which exposes several internal hydrophobic residues and part of the heme to solvent. The "cleft-opened" conformation appears to be identical to one observed by Storch and Daggett in a previously reported MD simulation of bovine Mc cyt b_5 (*38*). Subsequent studies with rat OM cyt b_5 mutants in which Ala-18, Ile-32, and Leu-47 have been replaced with the corresponding residues found in bovine Mc cyt b_5 revealed that the stability and tendency to lose heme correlate well with the degree to which the hydrophobic network is maintained. This conclusion is supported by a 2.0 Å crystal structure of the A18S/l47R/I32L triple mutant of rat OM cyt b_5, which shows that the hydrophobic network has been completely eliminated. Comparison of this crystal structure with those of the wild-type rat OM and bovine Mc proteins has also permitted us to identify some key structural differences between the rat OM cyt and bovine Mc proteins, which contribute to their contrasting preferences for binding hemin. Mc cytochromes b_5 favor isomer A, whereas rat OM cyt b_5 favors isomer B.

EXPERIMENTAL PROCEDURES

Protocols used for standard procedures such as plasmid isolations, transformations, ligation, and restriction endonuclease reactions were those published by Sambrook et al. (*39*). Recombinant rat liver OM cyt b_5 and the site-directed mutants studied in this work were expressed in *Escherichia coli* and purified as described previously (*23*). Single-stranded oligonucleotides were synthesized by the Recombinant DNA/Protein Facility at Oklahoma State University.

Site-Directed Mutagenesis. The recombinant plasmid MRL1 (*23*) and the transformer site-directed mutagenesis kit (Clontech) were used to obtain a gene coding for the A18S/L47R double mutant of rat OM cyt b_5. The sequences corresponding to the selection primer (*Afl*III to *Bgl*II) and mutagenic primers designed to introduce the A18S and L47R mutations follow: 5′-GGGGATAACGCAGGAAAGAACATGTGAGCAAAAGGCC-3′; 5′-GCGAAACGTAACACCTCTGAAGAAACCTGGATGG-3′; 5′-CGGCGAAGAAGTTCTGCGCGAACAGGCGGG-C-3′. The underlined codons represent mismatches introduced to generate the mutations. The PBS+ plasmid harboring the gene coding for the A18S/L47R double mutant was excised by digestion with the restriction endonucleases *Bam*HI and *Nde*I and then purified by electrophoresis. The 300 base pair gene was then cloned into the expression plasmid pET11a (*40*) and the recombinant pET plasmid transformed into BL21(DE3) *E. coli* cells for subsequent protein expression. The recombinant pET 11a plasmid (MRL2) (*23*) and the QuikChange site-directed mutagenesis kit (Stratagene) were used to construct the I32L mutant. The A18S/L47R/I32L triple mutant was constructed from the recombinant pET 11a plasmid harboring the gene coding for the A18S/L47R double mutant. The sequences corresponding to the mutagenic primers designed to introduce the I32L mutation are 5′-GGCCGTGTTTACGATCTGACCCGTTTCCTGTCTGAAC-3′ and 5′-GTTCAGACAGGAAACGGGTCAGATCGTAAACACGGCC-3′. The recombinant constructs were transformed into *E. coli* XL1-blue competent cells for amplification and subsequent sequencing. Once the sequence was established, the recombinant plasmids were transformed into *E. col*i BL21(DE3) cells for protein expression.

^{1}H NMR Spectroscopy. ^{1}H NMR spectra were recorded on Varian Unity Inova NMR spectrometers operating at 399.97 and 598.658 MHz, ^{1}H frequency. Protein solutions were exchanged with perdeuterated sodium phosphate buffer ($\mu = 0.1$ M, pH 7.0, not corrected for the isotope effect) in order to obtain a volume of 0.8 mL and a final concentration of ~3 mM. Spectra were acquired with water presaturation by accumulating 256 scans over a 30 kHz spectral width, 16K data points, and a relaxation delay of 2 s. Rate constants for heme−isomer interconversion were obtained by monitoring the time-dependent changes in the areas under the heme resonances corresponding to isomers A and B. The data were analyzed in terms of a reversible first-order reaction as described previously (*32*, *41*). In short, the heme interconversion reaction can be represented by eq 1 and the change in concentration of isomer A as a function of time is given by eq 2. If $[A]_0$ and $[B]_0$ are the concentrations of heme

$$A \underset{k_{-1}}{\overset{k_1}{\rightleftharpoons}} B \tag{1}$$

$$d[A]/dt = k_1[A] + k_{-1}[B] \tag{2}$$

isomer A and heme isomer B at time zero and $[A]_{eq}$ and $[B]_{eq}$ represent the equilibrium concentrations, eq 3 is readily obtained, which can be integrated to give eq 4. A plot of the

$$d[A]/dt = (k_1 + k_{-1})([A]_{eq} - [A]) \tag{3}$$

$$\ln\{[A] - [A]_{eq}/[A]_0 - [A]_{eq}\} = -(k_1 + k_{-1})t \tag{4}$$

term $\ln\{[A] - [A]_{eq}/[A]_0 - [A]_{eq}\}$ vs time should be linear with slope $-(k_1 + k_{-1})$. The equilibrium constant $K_{eq} = k_1/k_{-1}$ is obtained from the NMR spectrum when the heme interconversion reaction has reached equilibrium.

Thermal Denaturation Studies. Thermal denaturation experiments were performed on a Kontron UVIKON 9410 spectrophotometer outfitted with a thermostated cell compartment. Temperature was controlled by a VWR Scientific Model 1140A constant temperature circulator and monitored within the cell using an Omega Model HH200 thermometer with a T thermocouple (±0.2 °C). Sample concentration ranged from 3 to 5 μM in 50 mM potassium phosphate buffer, pH 7.0. The temperature was increased in approximately 5 °C increments, and samples were equilibrated for 15 min after reaching each desired temperature. The melting temperature (T_m) was determined from the first derivative of a plot of Soret band absorbance at 412 nm (λ_{max}) vs temperature.

Chemical Denaturation Studies. Stock solutions of guanidinium chloride (GdmCl; Aldrich) were prepared in 50 mM potassium phosphate buffer, pH 7. To eliminate potential errors in weighing of the hygroscopic GdmCl, stock solution concentrations were determined from measurements of the solution refractive index (*42*). A minimum of 15 solutions was used in each denaturation experiment. Solutions with final protein concentrations of 2−3 μM and GdmCl concentrations ranging from 0 to 5 M were maintained at 25 °C for 20 h before fluorescence and UV/vis spectra were recorded. The fluorescence intensity of each sample at 340 nm was recorded on a PTI QuantaMaster luminescence spectrometer, with excitation at 280 nm. Temperature was controlled by a VWR Scientific Model 1140A constant temperature circulator and monitored within the cell using the Omega Model HH200 thermometer described above. Each data point represents an average of five to seven scans. For each sample, a spectrum of a suitable blank solution was subtracted. UV/vis spectra were recorded at 25 °C using the instrument described above. Data were analyzed by the standard method for a two-state denaturation (*42*).

Hemin Transfer Experiments. Removal of heme from horse skeletal muscle myoglobin (Calbiochem) was accomplished using the method of Teale (*43*). Apomyoglobin (apoMb) concentrations were estimated using an extinction coefficient of 16.0 mM^{-1} cm^{-1} at 280 nm (*44*). For each hemin transfer experiment, a 1.0 mL solution of apoMb (12−15 μM) in 50 mM sodium citrate/sodium phosphate buffer was equilibrated at 21 °C in a 1.0 cm cuvette in the UV/vis spectrophotometer. A solution of cyt b_5 prepared in the same buffer (5 μL; final concentration 5−6 μM) was added to the apoMb solution. Continuous measurements of the absorbance at 406 nm were initiated about 20 s from time of addition of cyt b_5. The rate constants for hemin transfer at pH 5.2 were calculated from the initial rate data, using the exponential equation for a first-order reaction (eq 5). ΔA_t is the change in absorbance at time t, ΔA_{eq} is the change in absorbance at equilibrium, and k equals the rate constant for hemin transfer.

$$\Delta A_t = \Delta A_{eq}(1 - e^{-kt}) \tag{5}$$

ΔA_{eq} values at equilibrium were calculated using $\epsilon_{406} = 151$ mM^{-1} cm^{-1} for holoMb and $\epsilon_{406} = 122$ mM^{-1} cm^{-1} for holocyt b_5. These values are based on Soret band λ_{max} values reported in the literature for Mb (*45*) and cyt b_5 (*23*).

Crystallization and X-ray Diffraction Data Collection. Recombinant A18S/L47R/I32L was purified as described above. The protein was incubated at 60 °C in order to achieve the thermodynamically favored isomer ratio A:B = 1:4. The integrity of the protein was checked by ^{1}H NMR and electronic absorption spectroscopy and then exchanged into a buffer containing 20 mM Tris, pH 7.8, and 0.2% NaN_3 in order to initiate crystal growth experiments. Crystals were grown in vapor diffusion plates at 5 °C from hanging drops of the protein solution previously mixed 1:1 by volume with the reservoir solution containing 27% (w/v) poly(ethylene glycol) (MW 8000, PEG 8K), 0.2 M magnesium acetate, and 0.1 M PIPES, pH 6.5. The typical size of the crystals obtained with this system was approximately 0.2 mm × 0.2 mm × 0.3 mm. A single crystal was equilibrated with a solution similar to that contained in the reservoir solution (see above) but containing 36% (w/v) PEG 8K, flash-cooled in a stream of nitrogen gas to a temperature of approximately 100 K, and used for data collection. X-ray diffraction data were collected with a MAR345 image plate system installed on a Rigaku RU-43R X-ray generator equipped with an Osmic mirror. Raw data were processed using the program suite HKL (*46*). A complete data set was collected up to 2.0 Å resolution.

Structural Determination and Refinement. Molecular replacement calculations were performed using a model of our previously determined rat OM cyt b_5 crystal structure (PDB code: 1B5M) with the program AmoRe (*47*). One crystallographic asymmetric unit contains four cyt b_5 molecules with 44% solvent content. The initial R-factor and I_{obs}/I_{calc} correlation after the molecular replacement search

and prior to refinement were 0.36 and 0.7, respectively. Refinement was carried out using the program CNS (V.1.0) (*48*) with 6% of the total reflections randomly selected prior to the refinement and used to monitor the free *R* factor. Simulated annealing (from 5000 K) was used at the initial stage of the refinement to reduce bias of the template model. The graphic programs FRODO (Turbo) (*49*) and O (*50*) were used for interactive modeling. Noncrystallographic symmetry restriction was applied in the early stage of refinement. No solvent molecules were added to the model until the working *R*-factor was reduced to below 0.25. A bulk solvent correction and an isotropic overall *B*-factor refinement were applied throughout the refinement. In the final refined model, no backbone ϕ, ψ torsion angle pair is located in the disallowed region of the Ramachandran plot, and 98% of the residues are within either the most favored or the additionally allowed regions, as defined by PROCHECK (*51*). Coordinates of the crystal structure corresponding to the A18S/I32L/L47R mutant of rat OM cyt b_5 reported here have been deposited in the Protein Data Bank with accession code 1ICC.

Molecular Dynamics Simulations. Molecular dynamics simulations were performed using the program CHARMM (version 26) (*52*), with the version 22 all-atom protein topology and parameters (*53*). The initial protein structures were obtained from the X-ray coordinates deposited in the Protein Data Bank: file 1CYO for bovine Mc cyt b_5 (*27*) and file 1B5M for rat OM cyt b_5 (*26*). Residues 89−93 in bovine Mc cyt b_5 and residues 1−2 in the rat OM protein were not visible in the electron density maps and were thus omitted in the simulations. The simulated structures thus included 88 residues (1−88 from the sequence in 1CYO) for Mc cyt b_5 and 84 residues (3−86 from the sequence in 1B5M) for rat OM cyt b_5.

The missing hydrogen atoms were built in with the HBUILD module of CHARMM (*54*). To generate systems that were neutral overall and corresponded to solutions with ionic strengths close to the physiological value of 0.15 M, counterions were added using the program SOLVATE 1.0 (*55*). A total of 21 counterions (16 Na^+ and 5 Cl^-) were added to rat OM cyt b_5 and 22 counterions (15 Na^+ and 7 Cl^-) to bovine Mc cyt b_5. The cytochromes with their counterions were immersed in a truncated octahedral water cell, constructed by cutting off corners from a cube of side 62.2864 Å (*56*). After water molecules overlapping the proteins and counterions were deleted, the simulation cells contained 3460 water molecules for bovine Mc cyt b_5 and 3505 water molecules for rat OM cyt b_5. For each system the solvent and counterions were allowed to equilibrate for 100 ps in the presence of the fixed protein. This was followed by a brief energy minimization and a 100 ps equilibration of the whole system. Finally, a 1 ns molecular dynamics (MD) trajectory was generated for each of the systems.

The equilibration and trajectory phases of the calculation were carried out by MD simulations at constant pressure (1 atm) and constant temperature (300 K), under periodic boundary conditions. The leapfrog integrator was used (*57*) with a 2 fs time step, and SHAKE constraints were applied to all bonds involving hydrogen atoms (*58*). The Langevin piston method (*59*) was employed to maintain a constant pressure and the Hoover thermostat to maintain constant temperature (*57*). The particle-mesh Ewald (PME) method was employed in calculation of electrostatic interactions to avoid truncation of these long-range forces (*56*, *60*). The simulations were carried out on the SGI ORIGIN 2400 supercomputer at the Center for Advanced Scientific Computing at the University of Kansas. A 1 ns simulation of a solvated cyt b_5 system with PME treatment of electrostatics took about 40 CPU days on this computer.

RESULTS AND DISCUSSION

Molecular Dynamics Simulations. The heme-binding domain of cyt b_5 has been described as containing two cores. Core 1 comprises a four α-helical bundle that forms a cavity where the heme cofactor is located. Core 2, which consists of two short α-helices and a four-stranded β-sheet, is thought to be structurally independent of core 1. In fact, experimental (*61*) and theoretical (*62*) studies have shown that removal of heme from the protein has little effect on the structure of core 2. In contrast, loss of heme is accompanied by increased mobility and substantial loss of secondary structure in core 1. Hence, the structural integrity of core 1 is strongly dependent on protein−heme interactions.

In molecular dynamics (MD) simulations of bovine Mc cyt b_5, Storch and Daggett (*38*) observed time-dependent formation of a large cleft which exposes portions of the protein interior and of heme to the solvent. This cleft-opened intermediate was proposed to lie along the pathway of protein denaturation (*63*). As a means of elucidating structural explanations for the markedly different stabilities of the heme-binding domains of Mc and OM cytochromes b_5, we have performed an independent MD simulation of bovine Mc cyt b_5 as well as the first MD simulation of the rat OM isoform. The X-ray crystal structure coordinates of bovine Mc cyt b_5 (PDB accession code 1CYO) and of rat OM cyt b_5 (PDB accession code 1B5M) were used as starting points for these 1 ns length simulations. Explicit water molecules were included in the calculations, sodium and chloride ions were introduced to create solutions with a physiologically relevant ionic strength (0.15 M), and long-range electrostatic forces were accounted for through the use of Ewald summation (*56*), under conditions of constant temperature and pressure.

Bovine Mc Cyt b_5. The results obtained from our MD simulation of bovine Mc cyt b_5 are summarized in Figure 3. The time axis in all plots is split into two segments, an equilibration phase of 100 ps followed by the trajectory phase 1000 ps in length. During the equilibration phase, the protein in its crystal structure conformation is allowed to adjust to the water and counterion environment. Figure 3, panel A, reports time-dependent changes of backbone atom positions for residues 4−84 relative to their starting positions in the crystal structure. These data reveal a small change (∼0.6 Å) during the equilibration phase of the calculation. Little additional change is observed during the trajectory phase, and atomic fluctuations during this phase are small (∼0.4 Å). Hence, the motions of the microsomal protein can be described as small fluctuations centered around a stable structure represented by the X-ray crystal structure.

The data in Figure 3B reveal that the backbone atom positions of residues 49−51 deviate by 4−5 Å from their positions in the X-ray crystal structure. These deviations are significantly larger than the average deviations indicated in Figure 3A. The relatively large rms deviations observed for

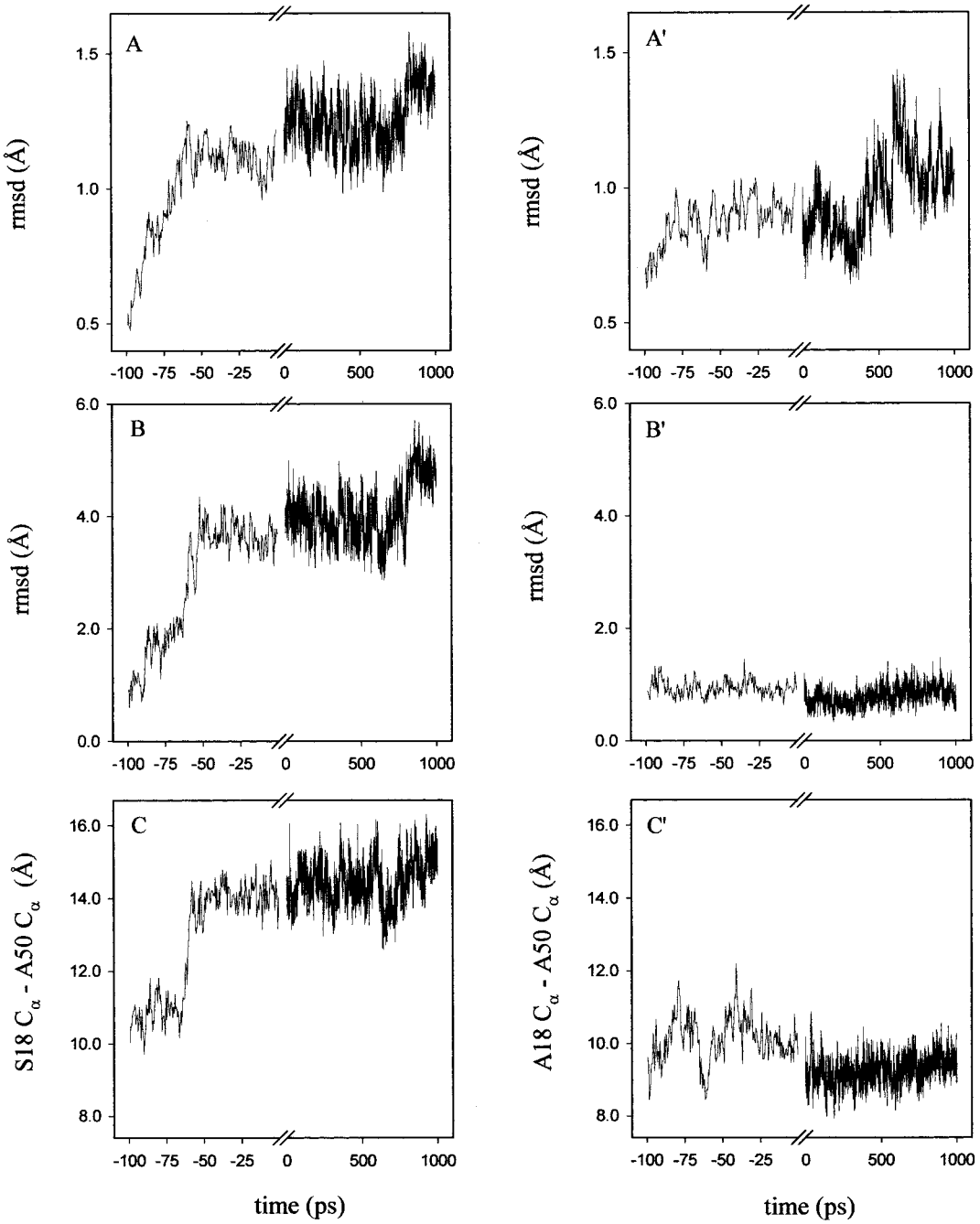

FIGURE 3: Summary of results obtained from molecular dynamics simulations of bovine Mc cyt b_5 (panels A, B, and C) and rat OM cyt b_5 (panels A′, B′, and C′). The time axis in all plots is divided in two segments, a 100 ps long equilibration time, where the starting structure is allowed to equilibrate in water in the presence of counterions, followed by a 1000 ps long trajectory segment. (A) Time-dependent rms deviations of backbone atom positions (residues 4−84) relative to their corresponding position in the starting X-ray structure of bovine Mc cyt b_5. (B) Time-dependent rms deviations observed for the backbone atom positions of residues 49−51 in bovine Mc cyt b_5. (C) Time-dependent variations in the distance between the C_α carbons of Ser-18 and Ala-50 in bovine Mc cyt b_5. (A′) Time-dependent rms deviations observed for the backbone atom positions of residues 3−80 in rat OM cyt b_5, relative to its X-ray crystal structure. (B′) Time-dependent rms deviations observed for residues 49−51 in rat OM cyt b_5. (C′) Time-dependent variations in the distance between the C_α carbons of Ala-18 and Ala-50 in rat OM cyt b_5.

residues 49−51 result from a structural transition in this region that occurs approximately 40 ps after commencing the equilibration phase (Figure 3B). Residues 49−51 are located on the protein surface and are involved in contacts with neighboring proteins in the crystal structure. Hence, such a large change in conformation is not altogether surprising.

Comparing the crystal structure of the protein (Figure 4A) with the structure observed during the trajectory phase of our calculation (Figure 4B) reveals that the conformational change involving residues 49−51 results in the opening of a cleft. This cleft is qualitatively identical to the one observed by Storch and Daggett in their MD simulation of bovine Mc cyt b_5 (compare Figure 6 in ref *38*). In our simulation, however, the protein remains in the cleft-opened conformation throughout the entirety of the 1000 ps trajectory, rather than oscillating between the "cleft-opened" and "cleft-closed" forms as observed by Storch and Dagget (*38*). The structural transition exposes several internal residues (gold and light blue in panels A and B in Figure 4) to the aqueous environment. Opening of the cleft is also revealed by a

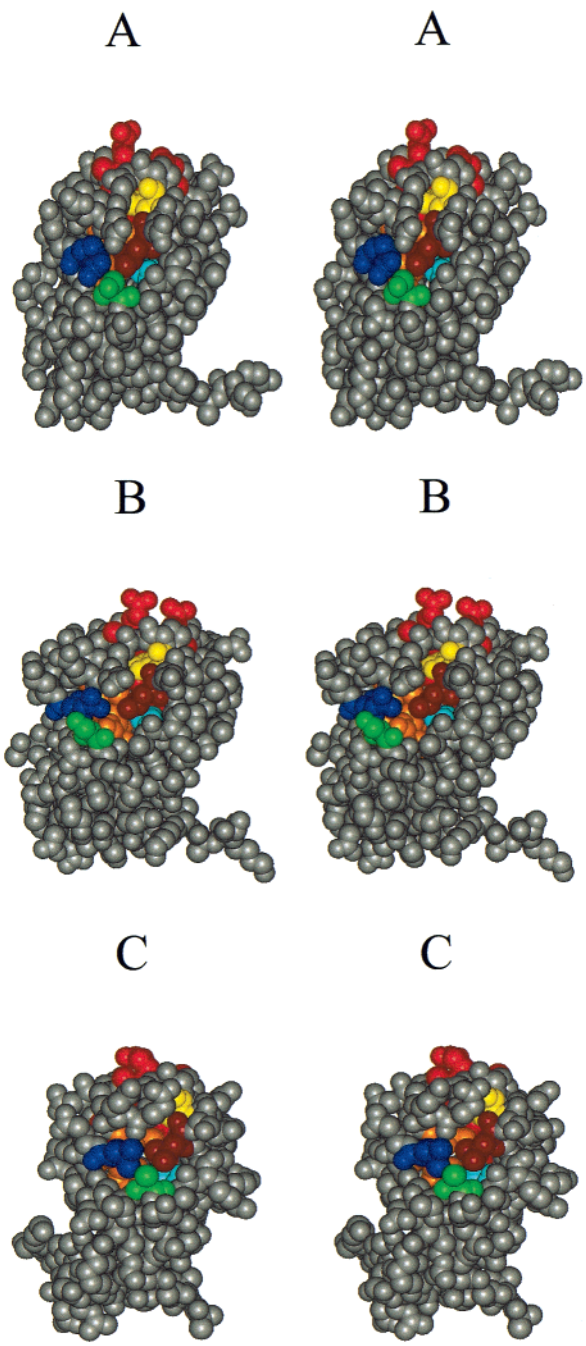

FIGURE 4: (A) Space-filling stereo representation of the X-ray structure of bovine Mc cyt b_5. (B) Space-filling stereo representation of bovine Mc cyt b_5 at the end of the MD simulations, i.e., 1000 ps trajectory time in Figure 3A. (C) Space-filling stereo representation of the structure of rat OM cyt b_5. In all structures heme is in red, axial ligands (His-39 and -63) are in yellow, Leu-36 is in brown, residue 18 is in green, residue 32 is in light blue, and residue 47 is in blue. Internal residues that become exposed upon opening of the cleft are in gold except for Leu-32, which is light blue.

substantial increase in distance between the residues in the 49−51 loop (located in core 2) and a number of residues in core 1. This is illustrated in Figure 3C, which reports time-dependent changes in distance between the C_α carbon atoms of Ser-18 (core 1) and Ala-50 (core 2). This distance increases from ∼11 to ∼14 Å approximately 40 ps after starting the equilibration phase of our calculations. Thereafter, the distance remains centered at approximately 14 Å (the distance observed in the crystal structure is ∼9.4 Å). In comparison, the distance between the hydroxyl hydrogen of Ser-18 and a methyl hydrogen of Ala-50 during the MD simulations of Storch and Daggett oscillates between approximately 9.4 Å (cleft closed) and 15 Å (cleft opened).

Although the cleft-opened conformation seen during the calculations of Storch and Daggett is reproduced during our calculations, it is interesting to point out that the cleft-opened conformation is acquired at approximately 40 ps in the equilibration phase of our calculations (see Figure 3B). Our calculations also show that this conformation is maintained during the entire trajectory. In contrast, the calculations of Storch and Daggett showed that the protein oscillates between the opened and closed conformations during their trajectory. The fact that details of the simulation results differ between our study and that of Storch and Daggett is not surprising due to numerous differences in methodology, including force fields employed, use of cutoffs, presence of counterions, and boundary conditions (constant volume in ref *38* vs constant pressure here). Nevertheless, it is highly satisfying that the general prediction of the existence of two conformers of Mc cyt b_5 in solution is reproduced in calculations performed under such different conditions.

Rat OM Cyt b_5. The results obtained from our MD simulation of rat OM cyt b_5 are summarized in Figure 3, panels A′, B′, and C′. As with the Mc isoform, the time axis has been split into an equilibration phase of 100 ps and a trajectory phase of 1000 ps. Figure 3A′ shows that residues 3−80 in rat OM cyt b_5 remain very close to their starting crystal structure positions during the MD simulations (rmsd ∼0.6 Å). It can also be seen from Figure 3A′ that the average atomic fluctuations in rat OM cyt b_5 (∼0.4 Å) are small and comparable to those observed for bovine Mc cyt b_5 (Figure 3A). In stark contrast to the observations made with the Mc protein, however, residues 49−51 in rat OM cyt b_5 do not undergo significant changes in position either during the equilibration phase of our calculation or during the 1000 ps length simulation. Atomic fluctuations of these residues are similar to the values for the overall protein (compare panels A′ and B′ in Figure 3) and smaller than observed for residues 49−51 in bovine Mc cyt b_5 (compare panels B and B′ in Figure 3). Finally, it is evident from Figure 3C′ that, during the equilibration and trajectory phases of the rat OM cyt b_5 MD simulation, the distance between the C_α carbons of residues 18 and 50 (8.4 Å) does not deviate from that observed in the crystal structure. As noted above, the distance between these residues increases significantly during the "cleft-opening" process in bovine Mc cyt b_5 (Figure 3C). Taken together, the data indicate that rat OM cyt b_5 does not adopt the cleft-opened conformation.

Relationship between Amino Acid Sequence, Cleft Dynamics, and Structural Stability in Mc and OM Cytochromes b_5. The striking differences observed in the MD simulations of bovine Mc cyt b_5 and rat OM cyt b_5 suggested to us that the enhanced stability of the rat OM protein and its greater kinetic barrier to hemin release and reorientation may be related to its inability to adopt the cleft-opened conformation. Consequently, we decided to explore the structural properties that may inhibit opening of the cleft in rat OM cyt b_5. This process was initiated by comparing amino acid sequences of the heme-binding domains of several mammalian Mc cytochromes b_5 with the corresponding sequence of rat OM cyt b_5 (see Figure 1). Subsequent comparison of the X-ray

crystal structures of the two proteins allowed us to identify local structural variations resulting from the amino acid sequence differences that might contribute to their markedly dissimilar biophysical properties. This analysis led to a number of interesting observations. For example, residues Ser-18 and Arg-47 of bovine Mc cyt b_5 are located in cores 1 and 2, respectively. In the X-ray crystal structure of bovine Mc cyt b_5 (see Figure 4A), the side chains of Ser-18 (green) and Arg-47 (blue) form a hydrogen bond. Opening of the cleft described by Daggett et al. (*38*, *63*) is accompanied by breaking of the hydrogen bond between Ser-18 and Arg-47 and a change in orientation of the Arg-47 side chain, which exposes portions of the hydrophobic protein interior to the aqueous environment (Figure 4B). It is noteworthy that Ser-18 and Arg-47 are invariant in all mammalian cytochromes b_5 whose sequences have been determined to date (Figure 1). In stark contrast, positions 18 and 47 in rat OM cyt b_5 are occupied by Ala and Leu, respectively. The result of this difference in protein sequence is replacement of an amino acid pair which can form a hydrogen bond (blue and green in Figure 4A) with a pair that can only engage in hydrophobic interactions. The hydrophobic packing between Ala-18 and Leu-47 in rat OM cyt b_5 can be appreciated from the stereoview of the crystal structure shown in Figure 4C, where Ala-18 and Leu-47 are shown in green and blue, respectively. As discussed below, Ala-18 and Leu-47 of rat OM cyt b_5 participate in a hydrophobic cluster that is much more extensive than the corresponding cluster in the bovine Mc structure.

A second, more subtle difference in sequence between rat OM and the Mc cytochromes b_5 occurs at position 32. In all Mc cytochromes b_5 sequenced to date, residue 32 is Leu (see Figure 1). Leu-32 in the X-ray crystal structure of bovine Mc cyt b_5 is highlighted in light blue (Figure 4A). In rat OM cyt b_5 this position is occupied by Ile (light blue in Figure 4C). Leu-32 in bovine Mc cyt b_5 is one of the residues which experiences an increase in solvent exposure upon opening of the cleft observed in the MD simulations (see Figure 4B). The side chains of Ile and Leu are both hydrophobic and contain the same number of carbon atoms. However, their different shapes result in strikingly different hydrophobic packing arrangements in the vicinity of Leu-32 in bovine Mc and Ile-32 in rat OM cyt b_5. For instance, it is evident from Figure 4C that the γ-methyl group of Ile-32 (light blue) in rat OM cyt b_5 engages in hydrophobic interactions with one of the methyl groups in the side chain of Leu-36 (brown). Leu-36, in turn, is involved in an additional hydrophobic interaction with the side chain of Leu-47 (blue), which is also involved in a hydrophobic interaction with Ala-18 (green). In comparison, there is no hydrophobic interaction between Leu-32 and Leu-36 in bovine Mc cyt b_5. In fact, the hydrophobic packing in this region of bovine Mc cyt b_5 (cleft-closed form) is limited to an interaction between the side chains of Leu-36 and Arg-47 (see Figure 4A).

It is therefore possible to postulate that the extended hydrophobic cluster comprising the side chains of Ala-18, Ile-32, Leu-36, and Leu-47 in rat OM cyt b_5 (see Figure 4C) contributes to the inability of the rat OM protein to adopt a cleft-opened conformation as readily as bovine Mc cyt b_5. As noted in the previous section, opening of the cleft in bovine Mc cyt b_5 results in greater access of water to the interior of the protein (see Figure 4B). Hence, the inability of rat OM cyt b_5 to adopt the cleft-opened conformation may contribute to its greater stability toward chemical and thermal denaturation. To probe this possibility, we performed a study in which the structure of bovine Mc cyt b_5 was used as a template for designing mutants of rat OM cyt b_5. These mutagenesis studies were carried out with the aim of studying the roles of residues Ala-18, Leu-47, and Ile-32 in stabilizing the fold of rat OM cyt b_5 with respect to the Mc isoforms. The results of these experiments are described below.

Probing the Relationship between Cleft Dynamics and Protein Stability. To probe the influence of the hydrophobic network encompassing residues 18, 32, 36, and 47 on the stability of rat OM cyt b_5, we prepared three mutants of the protein. In one mutant, Ile-32 was replaced by Leu, the corresponding residue found in all Mc cytochromes b_5. An A18S/L47R double mutant of rat OM cyt b_5 was prepared in order to replace the hydrophobic interaction between Ala-18 and Leu-47 in rat OM cyt b_5 with the hydrogen-bonding interaction between Ser-18 and Arg-47 observed in bovine Mc cyt b_5. Finally, we have also prepared the A18S/L47R/I32L triple mutant of rat OM cyt b_5, to eliminate the hydrophobic packing characteristic of the mitochondrial protein and introduce the structural microenvironment characteristic of the Mc isoforms.

The consequences of altering the hydrophobic microenvironment of rat OM cyt b_5 so that it closely resembles the corresponding microenvironment of the Mc isoforms were investigated by comparing the stability of the mutant proteins toward thermal and chemical denaturation. Thermal denaturation experiments were performed using UV/vis spectroscopy, monitoring temperature-dependent changes in absorbance of the Soret band (λ_{max} 412 nm). Analysis of a plot relating absorbance at 412 nm vs temperature (Figure 5A) provides the midpoint of thermal denaturation (T_m). T_m values obtained in these experiments (summarized in Table 1) indicate that the stability of the mutant proteins correlates with the degree of perturbation of the extended hydrophobic patch under investigation. For instance, in agreement with the expectation that the I32L mutation should cause the smallest perturbation of the hydrophobic patch, the midpoint of thermal denaturation of this mutant is only ~1 °C lower than that of wild-type rat OM cyt b_5. Substitution of Ala-18 and Leu-47 for Ser and Arg, respectively, creates a larger perturbation of the hydrophobic patch by eliminating the hydrophobic packing between Ala-18, Leu-47, and Leu-36. In agreement with the anticipated extent of perturbation of the hydrophobic patch, the midpoint of thermal denaturation of the A18S/L47R double mutant is 4 °C lower than for the wild-type protein. Introducing the I32L mutation into the A18S/L47R double mutant, yielding the A18S/L47R/I32L triple mutant, results in a small additional destabilization (~1.5 °C). Hence, the triple mutant is the least stable of the proteins studied. Consistent with this experimental observation, the X-ray crystal structure of the A18S/L47R/I32L triple mutant (discussed below) reveals that the extended hydrophobic patch has been eliminated, as predicted. It is important to point out that the bovine Mc protein is considerably less stable (see Table 1) than the rat OM triple mutant. Clearly, additional structural differences between rat OM cyt b_5 and the Mc isoforms contribute to the greater stability of the rat OM protein.

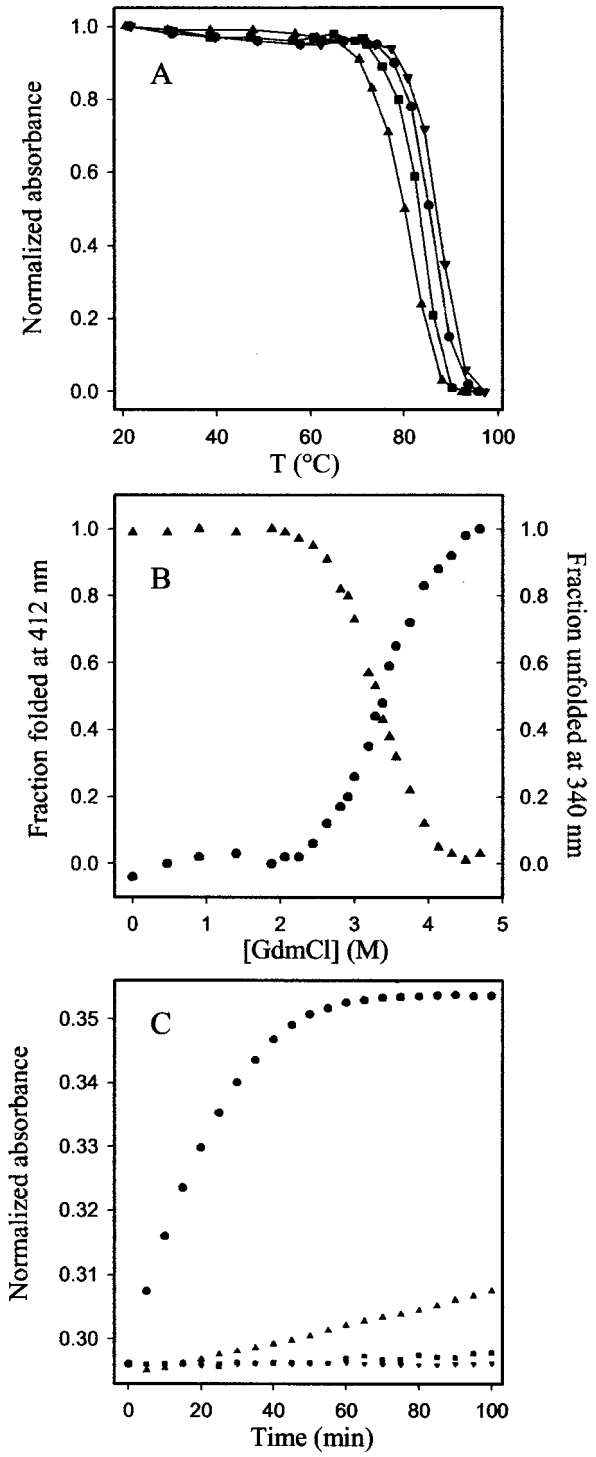

FIGURE 5: (A) Plots of normalized absorbance at 412 nm (Soret band λ_{max}) vs temperature for wild-type rat OM cyt b_5 (▼) and the I32L (●), A18S/L47R (■), and A18S/L47R/I32L (▲) mutants. Data were acquired in 50 mM potassium phosphate buffer, pH 7.0, and normalized by setting the intensity of the Soret band of each 20 °C spectrum to 1.0. (B) Data from GdmCl-induced chemical denaturation studies of the A18S/L47R/I32L triple mutant of rat OM cyt b_5. Fractions of folded and unfolded protein were monitored by UV/vis (▲) and fluorescence (●) spectrophotometry. All measurements were performed at 25 °C in 50 mM potassium phosphate solution buffered to pH 7.0. (C) Data from hemin transfer experiments with bovine Mc cyt b_5 (●), wild-type rat OM cyt b_5 (▼), and the A18S/L47R (■) and A18S/L47R/I32L (▲) mutants. Although transfer was normally monitored for 10 h, data are only shown for the first 100 min of each experiment. All data were recorded in 50 mM sodium phosphate/sodium citrate buffer, pH 5.2, and at 21 °C (bovine data were recorded at 25 °C).

In work reported in a previous communication we probed the stability of wild-type rat OM cyt b_5 toward guanidinium chloride (GdmCl) mediated denaturation (*25*). In these experiments hemin loss was monitored by UV/vis spectroscopy while protein denaturation was followed by changes in the fluorescence intensity of Trp-22. The denaturation curves revealed that hemin loss and protein unfolding each occur as part of a single cooperative transition. Furthermore, the denaturation curves obtained by UV/vis or fluorescence spectroscopy yield identical midpoints of chemical denaturation (C_m). These observations were interpreted to mean that disruption of the hydrophobic core around Trp-22 (core 2) and of the hemin-binding domain (core 1) occur simultaneously. In other words, protein denaturation is concomitant with hemin release. To examine whether the mutations performed for the purposes of this study might have differentially affected these two processes, we performed chemical denaturation experiments with the single, double, and triple mutants described above. The results of these experiments are summarized in Table 1. A typical set of UV/vis and fluorescence data obtained for the A18S/L47R/I32L triple mutant is shown in Figure 5B. It is evident from this plot and from the midpoint values of chemical denaturation obtained by UV/vis and fluorescence spectroscopy (Table 1) that the mutations did not uncouple the hemin release and protein unfolding events. It is also noteworthy that the relative stability of the mutants, judged by their midpoint of chemical denaturation, parallels the relative stability observed by thermal denaturation. Furthermore, both thermal and chemical denaturation data demonstrate that the triple mutant of rat OM cyt b_5 is more stable than the bovine Mc protein. The results summarized in Table 1 clearly indicate that the stability of the studied proteins decreases in the following order: WT rat OM > rat OM I32L > rat OM A18S/L47R > rat OM A18S/L47R/I32L > bovine Mc cyt b_5.

Given the fact that the mutant proteins are less stable than wild-type rat OM cyt b_5, it was of interest to investigate whether the apoproteins would follow a similar trend. To this end, the stabilities of the apo forms of rat OM wild-type cyt b_5 and the corresponding A18S/L47R/I32L triple mutant were also examined by chemical denaturation. Protein unfolding in this case was monitored by changes in fluorescence of Trp-22 as a function of GdmCl concentration. C_m values determined for the wild-type (1.2 ± 0.2) and triple mutant (1.1 ± 0.2) apoproteins are the same within error, thus indicating that the mutations performed as part of this study have no measurable effect on stability of the proteins after hemin has been removed. Since the relative stability of the apoproteins has not been affected by the mutations, and because protein unfolding and hemin release are coupled events, we interpret the results to mean that the decreased stability of the mutant holoproteins originates from changes in hemin−polypeptide interactions that facilitate hemin release. To further investigate this possibility, we turned our attention to examining the effect of the mutations on hemin loss (see Table 1). This was accomplished by monitoring hemin transfer from the mutant proteins to apomyoglobin, using experiments based on a method previously developed for measuring hemin release from myoglobin mutants (*64*, *65*). In short, addition of about a 2-fold excess of apomyoglobin to a solution containing the appropriate OM cyt b_5 mutant should result in an increase in the absorbance

Table 1: Thermal Denaturation, Chemical Denaturation, and Hemin Transfer Data[a]

protein	T_m (°C)	C_m (M)		k_{-H} (h^{-1})	
		fluor	UV/vis	pH 6.8[b]	pH 5.2[b]
rat OM	87.0 ± 0.4	4.09 ± 0.05[c]	4.03 ± 0.02[c]	*d*	*d*
rat OM I32L	85.7 ± 0.1	3.93 ± 0.02	3.91 ± 0.01	*d*	*d*
rat OM A18S/L47R	83.3 ± 0.5	3.56 ± 0.03	3.52 ± 0.02	*d*	0.03 ± 0.01
rat OM A18S/I32L/L47R	81.8 ± 0.9	3.34 ± 0.02	3.33 ± 0.02	<0.01	0.10 ± 0.03
bovine Mc	73.1 ± 0.4[e,f]	2.99 ± 0.1[e,g]	3.05 ± 0.1[e,g]	0.52[h]	3.1[h]

[a] All data were recorded in 50 mM potassium phosphate buffer at pH 7.0, unless otherwise noted. [b] 50 mM sodium citrate/sodium phosphate buffer. [c] These correct our previously reported values (*25*). [d] Too slow to measure. [e] Residues −4 to 100, using the numbering scheme in Figure 1. [f] 5 mM MOPS buffer (*72*). [g] 30 mM MOPS buffer (*73*). [h] Tryptic fragment, corresponding to residues 3−84 in Figure 1 (*25*).

corresponding to holomyoglobin, if hemin is being transferred from holocyt b_5 to apomyoglobin. Once transfer is complete, the resultant electronic absorption spectrum should correspond to that of holomyoglobin.

We have recently reported that wild-type rat OM cyt b_5 does not transfer hemin to apoMb at pH values between 6.8 and 5.2. In striking contrast, hemin transfer from bovine Mc cyt b_5 to apoMb is complete in 6 h at pH 6.8 and in 1 h at pH 5.2 (*25*). The faster rate of hemin transfer observed for bovine Mc cyt b_5 at pH 5.2 is related to the fact that, at lower pH, protonation of the His side chains competes effectively with coordination of His to iron. As was observed with the wild-type protein, the I32L (single) and A18S/L47R (double) mutants are unable to transfer hemin to apoMb at pH = 6.8 (data not shown), and hemin transfer from the A18S/L47R/I32L triple mutant is exceedingly slow. At pH = 5.2, however, hemin transfer is observed for the A18S/L47R (double) and A18S/L47R/I32L (triple) mutants (see Figure 5C). Rate constants for hemin release, summarized in Table 1, reveal that the less stable of these two proteins (the A18S/L47R/I32L triple mutant) releases hemin more rapidly. Transfer of hemin from the triple mutant to apoMb is complete within about 8 h. Nonetheless, hemin transfer from both mutants is still considerably slower than measured for bovine Mc cyt b_5 at the same pH (*25*). The I32L single mutant, like the wild-type protein, does not release hemin at a measurable rate at pH 5.2. In fact, the electronic absorption spectra of these two proteins remain unchanged even after 10 h of incubation with apomyoglobin. This finding is consistent with the similar stabilities of the wild-type and I32L proteins discussed above. In summary, the results obtained from the hemin transfer experiments support our prediction that the relative stabilities of WT rat OM cyt b_5, the three mutants described herein, and bovine Mc cyt b_5 are related to their relative propensities to lose hemin.

X-ray Crystallography. An X-ray crystal structure (2.0 Å resolution) was obtained for the water-soluble domain (core 1 and core 2) of the rat OM cyt b_5 A18S/L47R/I32L triple mutant in order to obtain structural information regarding the microenvironment defined by residues Ser-18, Leu-32, and Arg-47. The crystal grew from a solution containing poly(ethylene glycol) as the precipitant, utilizing conditions similar to those employed to grow other crystal forms of rat OM and mutant cytochromes b_5 (*26*, *29*, *30*). The structure has been refined to an *R*-factor of 20.0%, with an R_{free} of 26.0%. The statistics of the diffraction data and refinement results are summarized in Table 2. There are four cyt b_5 molecules per crystallographic asymmetric unit cell. The root mean square (rms) deviations between the C_α atoms (residues 4−84) of each possible pair of protein molecules in the asymmetric unit cell range between 0.34 and 0.41 Å, thus indicating that the structures of the four independent protein molecules in the unit cell (A, B, C, and D) are essentially identical. The conformations of the amino termini of molecules A and B are well defined in the electron density map, while the first three residues in molecules C and D are mobile, since their crystal packing environments are different. The four protein molecules in an asymmetric unit cell can be arranged into a 2-fold symmetric tetramer. Two nonsymmetric dimers, AB and CD, are related by a local 2-fold rotation axis which is approximately parallel to the *a*−*b* plane of the crystal lattice and 42° from the *a* axis. The two monomers in a nonsymmetric dimer are related by a 133° rotation plus a 21 Å translation along the rotation axis. The rms deviation between the C_α atoms (residues 4−84) of the two dimers, AB and CD, is 0.59 Å, suggesting well-defined interactions between the two monomers. None of the three mutated residues is directly involved in the dimer interface or other crystal packing. The above-mentioned tetramers are packed through another local 2-fold symmetry, which is composed by a 180° rotation plus a 4 Å translation, in addition to crystallographic symmetries. Approximately 250 solvent molecules were modeled in the refined crystal structure, roughly about 0.7 solvent molecule per amino acid residue. Three of them were modeled as magnesium cations, which is present in the crystallization buffer.

Table 2: Data Collection and Refinement Statistics

(a) data statistics	
space group	$P2_12_12_1$
unit cell (Å)	$a = 39.9$
	$b = 51.3$
	$c = 167.4$
resolution (Å)	23.0−2.0
R_{merge} (%)	0.08 (0.53)[a]
no. of reflections	23878 (2324)
completeness (%)	98.6 (98.9)
(b) refinement statistics	
$R_{working}$ (%)	19.6 (for 20529 reflections)[b]
R_{free} (%)	24.0 (for 1494 reflections)[b]
no. of non-hydrogen atoms	
protein (including heme)	2941
solvent	162
rms deviation from ideal values	
bond length (Å)	0.014
bond angle (deg)	1.60
average *B*-factor (Å^2)	
protein	31.0
solvent	35.7

[a] Numbers in parentheses are the corresponding numbers for the highest resolution shell (2.1−2.0 Å). The highest resolution shell with R_{merge} below 20% is that corresponding to 2.5−2.4 Å. [b] Reflections with $|F_o| > 0.0$.

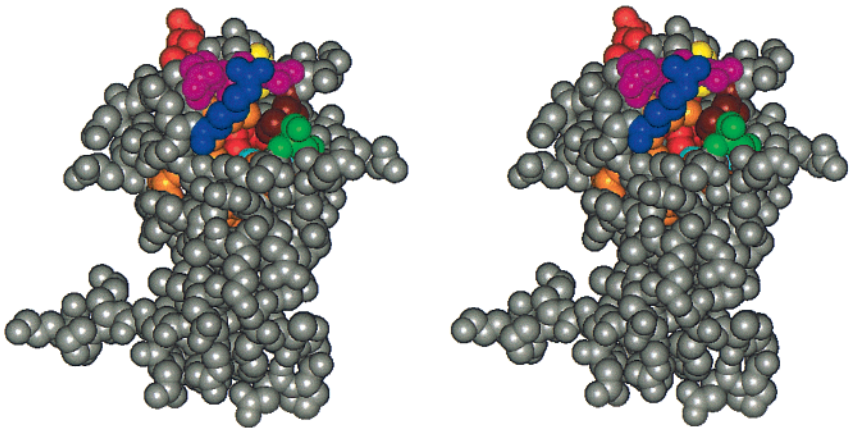

FIGURE 6: Stereoview obtained from the crystal structure coordinates of the A18S/L47R/I32L triple mutant of rat OM cyt b_5. Heme is in red, Arg-47 is in blue, Ser-18 is in green, Leu-32 is in light blue, and Leu-36 is in brown. This view of the structure demonstrates that the extended hydrophobic cluster created by Ala-18, Ile-32, Leu-36, and Leu-47 is absent in the structure of the triple mutant. The end result is enhanced exposure of internal residues to the aqueous environment.

The overall fold of the A18S/L47R/I32L triple mutant is indistinguishable from that of wild-type rat OM cyt b_5. All three mutated residues (18, 32, and 47) display good electron density, which structurally confirms the mutations. Among the mutated residues, the atoms in Leu-32 have lower than average *B*-factors in all four molecules. It is important to note that Leu-32 and Ser-18 in the triple mutant crystal structure adopt orientations essentially identical to those of Ser-18 and Leu-32 in bovine Mc cyt b_5. The side chain of Arg-47 in the triple mutant (blue in Figure 6), on the other hand, adopts a different orientation in the rat OM triple mutant. In bovine Mc cyt b_5, one NH_2 group on the guanidinyl side chain of Arg-47 forms a salt bridge with the carboxylate side chain of Glu-43. The other NH_2 group is situated close to the side chain hydroxyl group of Ser-18. In contrast, the guanidinyl group of Arg-47 in the triple mutant engages in salt bridge interactions with the side chain carboxylate groups of Glu-43 and Glu-44 (conserved in all mammalian cytochromes b_5; magenta in Figure 6). This difference in orientation, resulting from changes in the side chain χ_2, χ_3, and χ_4 torsional angles, no doubt reflects the inherent flexibility of the Arg side chain, coupled with its location on the protein surface. Note that the conformation of Arg-47 in the structure of the rat OM triple mutant reveals the presence of a deep cavity (Figure 6). The cavity exposes several internal residues (shown in gold), including Leu-32 (light blue), and a part of the heme (red) to the aqueous environment. Changing the conformation of the Arg-47 side chain in the structure of bovine Mc cyt b_5 so as to match that observed in the structure of the rat OM triple mutant reveals an essentially identical cavity. It is likely that the side chain of Arg-47 samples these two, and possibly other conformations in solution, hence periodically exposing the protein interior to the aqueous environment. Several of the residues experiencing increased solvent exposure when Arg-47 forms a salt bridge with Glu-43 and Glu-44 were also exposed when bovine Mc cyt b_5 switched from the cleft-closed to the cleft-opened form during MD simulations (compare Figures 4B and 6).

As discussed in the preceding paragraph, the side chain of Arg-47 can form a hydrogen-bonding interaction with Ser-18 or salt bridge interactions with Glu-43 and Glu-44. In this context, it is illustrative to analyze the microenvironment of residue 47 in rat OM cyt b_5. In the mitochondrial isoform position 47 is occupied by Leu, shown in blue in Figure 4C. Contrary to Arg-47 in the triple mutant protein, Leu-47 in rat OM cyt b_5 engages in hydrophobic interactions with Ala-18 (green in Figure 4C) and Leu-36 (brown). Leu-36 forms additional hydrophobic interactions with the α-methyl of Ile-32 (light blue), hence forming an extended hydrophobic patch that is absent in bovine Mc cyt b_5, and in the A18S/L47R/I32L triple mutant of rat OM cyt b_5. If Leu-47 were to adopt an alternate side chain conformation, it would lose its hydrophobic interactions with Ala-18 and Leu-36. In contrast to Arg-47 in the bovine protein, these lost interactions would not be compensated by stabilizing interactions with other nearby side chains. We therefore postulate that the side chain of Leu-47 is much less likely than Arg to frequently sample additional conformations in solution. As a result, the hydrophobic interactions between the side chains of Leu-47, Ala-18, and Leu-36 on the surface of the protein prevent the formation of a cavity that exposes internal residues to the aqueous environment. Consequently, it is possible to conclude that the loss of favorable hydrophobic interactions upon replacing Ala-18 and Leu-47 in the rat OM protein with Ser and Arg contributes significantly to the reduced stability and higher rate of hemin release exhibited by the A18S/L47R double mutant. Loss of additional hydrophobic interactions following change of Ile-32 for Leu contributes to even greater destabilization of the A18S/L47R/I32L triple mutant.

The Issue of Heme Isomerism. Wild-type rat OM cyt b_5 is heterogeneous as a result of heme being bound in two orientations related to each other by a 180° rotation about the porphyrin α−γ-meso axis (*23*, *66*) (see Figure 7). This is a well-known property of cytochromes b_5 and other hemoproteins where the heme center is not covalently attached to the polypeptide (*67*−*69*). The two orientations are denoted as A and B, where A is the predominant form in bovine Mc cyt b_5. The ratio of hemin orientations at equilibrium (A:B) differs widely among cytochromes b_5; for instance, it is 9:1 in bovine Mc, 20:1 in chicken Mc, 1.6:1 in rat Mc, and 1:1 in rat OM cyt b_5 (*23*, *32*, *68*−*71*). When apocytochromes b_5 are reconstituted with hemin, the resultant holoproteins are 1:1 mixtures of isomers A and B. As time proceeds, however, the ratio of isomer A to isomer B in all

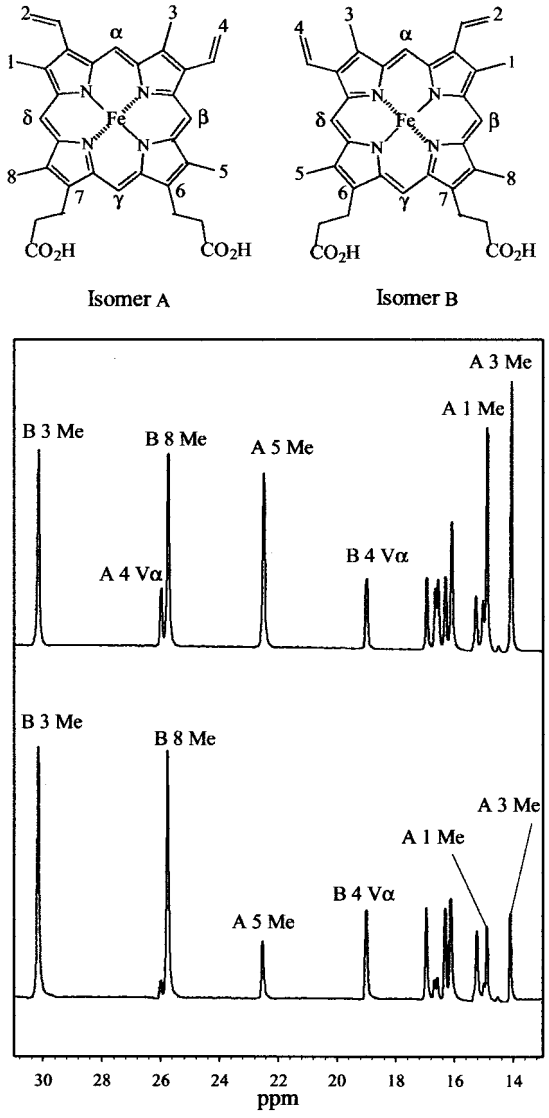

FIGURE 7: ^{1}H NMR spectra obtained from samples containing the A18S/L47R/I32L triple mutant of rat OM cyt b_5 after purification and exchange into deuterated buffer (top) and after incubation of the sample at 65 °C for 7 h (bottom).

Mc cytochromes increases until the equilibrium mixture has been attained. For example, isomer B in bovine Mc cyt b_5 is transformed into isomer A with a half-life of 13 h at pH 7.0 and 24 °C (*32*). In contrast, we recently reported that hemin in rat OM cyt b_5 is kinetically trapped at physiologically relevant temperatures (~37 °C) (*25*). In the same report we demonstrated that if rat OM cyt b_5 is heated to 65 °C for approximately 7 h, isomer A is converted into isomer B, resulting in an equilibrium mixture A:B = 1:1.2 (*25*). This finding provided the first example of a cytochrome b_5 where isomer B is thermodynamically favored.

The A18S/L47R/I32L triple mutant of rat OM cyt b_5 was prepared in order to test our hypothesis that residues Ala-18, Ile-32, Leu-36, and Leu-47 participate in an extended network of hydrophobic interactions that prevent the rat OM protein from adopting the cleft-opened conformation. The amino acids selected to replace Ala-18, Ile-32, and Leu-47 in rat OM cyt b_5 (Leu-36 is conserved in Mc and OM isoforms) were those found in the corresponding positions in the Mc cytochromes b_5 (see Figure 1). It was reasoned that introducing Ser-18, Leu-32, and Arg-47 into rat OM cyt b_5 would facilitate opening of the cleft, thereby endowing the A18S/L47R/I32L triple mutant of rat OM cyt b_5 with some of the characteristics typical of Mc cytochromes b_5. Consistent with this prediction, disruption of the hydrophobic network decreased the stability of the rat OM protein and increased the rate of hemin loss. It was therefore of interest to probe whether disrupting the hydrophobic packing in rat OM cyt b_5 would also exert an influence on the phenomenon of hemin orientational isomerism. This issue was addressed with the aid of ^{1}H NMR spectroscopy, and the findings obtained from these experiments are discussed below.

The high-frequency region of the A18S/L47R/I32L triple mutant NMR spectrum is shown in Figure 7, top trace. This spectrum is almost identical to the spectrum obtained from wild-type rat OM cyt b_5 (*23*, *25*, *66*), hence making hemin resonance assignments straightforward. The ^{1}H NMR spectrum of the A18S/L47R/I32L triple mutant was obtained after the protein was purified and exchanged into deuterated phosphate buffer. The hemin isomer ratio was evaluated by comparing the area under the peaks corresponding to heme methyl groups in the A and B isomers; the ratio was found to be A:B = 1:1. The ^{1}H NMR spectrum obtained after the A18S/L47R/I32L triple mutant had been incubated at 65 °C for 6 h, however, indicates that hemin orientational isomer ratio A:B = 1:4 has been achieved (Figure 7, bottom trace). No further changes are observed with longer heating, indicating that equilibrium has been reached. As noted above, the equilibrium A:B ratio observed for wild-type rat OM cyt b_5 after incubation at 65 °C for 7 h is significantly smaller (~1:1.2). Hence, the structural changes introduced into the triple mutant have resulted in greater energetic stabilization of isomer B.

Insight into the factors reponsible for this change in equilibrium isomer ratio came from the following observations: (1) the equilibrium A:B ratio observed for the A18S/L47R double mutant after incubation at 65 °C is identical to that observed for the wild-type protein (A:B = 1:1.2), and (2) the equilibrium ratio obtained for the I32L single mutant is the same as that observed for the A18S/L47R/I32L triple mutant (A:B = 1:4). These observations strongly suggest that residue 32 plays a key role in controlling the relative stability of isomers A and B in rat OM cyt b_5. This hypothesis is supported by side-by-side comparisons of the X-ray crystal structures of bovine Mc cyt b_5, wild-type rat OM cyt b_5, and the rat OM A18S/L47R/I32L triple mutant. However, residue 32 is only one of several nearby residues that act synergistically to dictate the relative stabilities of the hemin isomers. It is important to point out that the structure of the A18S/L47R/I32L triple mutant was obtained from a crystal grown from protein exhibiting a hemin isomer ratio A:B = 1:4 (see Experimental Procedures). Consequently, the hemin orientation in the X-ray crystal structure of the triple mutant (Figure 8A) corresponds to isomer B. In contrast, the heme active site in the structures of wild-type rat OM cyt b_5 (Figure 8B) and bovine Mc cyt b_5 (Figure 8C) corresponds to isomer A. The structure of the A18S/L47R/I32L triple mutant revealed that the side chain of Leu-32 (blue in Figure 8A) is located at the bottom of the heme-binding pocket, adopting an orientation essentially the same as that observed for Leu-32 in bovine Mc cyt b_5. The two δ-CH_3 groups on the isobutyl side chain are directed toward

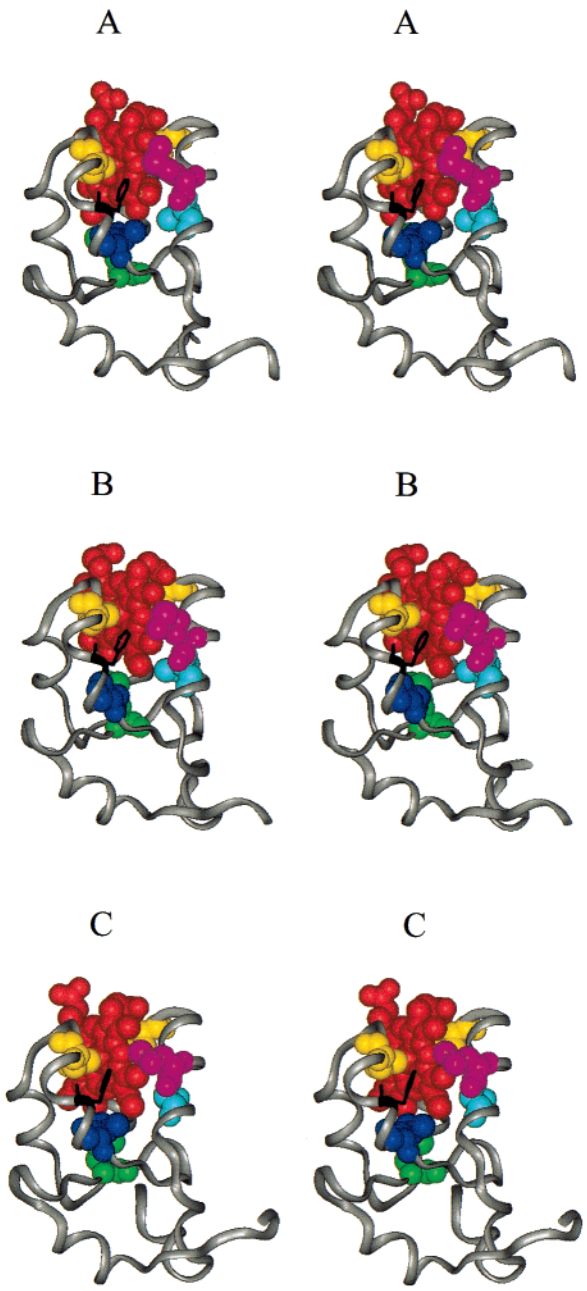

FIGURE 8: Stereoviews highlighting structural details in the region near heme methyl group 3 in the B isomer (B3Me), a position that is occupied by heme vinyl 2 in the A isomer (A2V). Structures corresponding to the two heme isomers obtained by rotating the heme molecule about the $\alpha-\gamma$-meso axis are shown in Figure 7. In all stereoviews, the heme is in red, the axial ligands (His-39 and His-63) are in yellow, and Phe-35 is in black with line rendering. (A) A18S/L47R/I32L mutant of rat OM cyt b_5. Leu-32 is in blue, Leu-71 is in light blue, Met-23 is in green, and Met-70 is in magenta. (B) Wild-type rat OM cyt b_5. Ile-32 is in blue, Leu-71 is in light blue, Met-23 is in green, and Met-70 is in magenta. (C) Bovine Mc cyt b_5. Leu-32 is in blue, Ser-71 is in light blue, Leu-23 is in green, and Leu-70 is in magenta.

the heme, coming within 3.9 and 4.2 Å of the heme methyl group (B3Me). In comparison, Ile-32 in the structure of wild-type rat OM cyt b_5 (blue in Figure 8B) adopts a side chain geometry which directs the lone δ-CH_3 group away from the heme. The side chain geometries of Ile-32 in wild-type rat OM cyt b_5 and of Leu-32 in the triple mutant are compared in Figure 9. The end result of the Ile-32 to Leu-32 mutation is a decrease in space at the bottom of the heme-binding pocket.

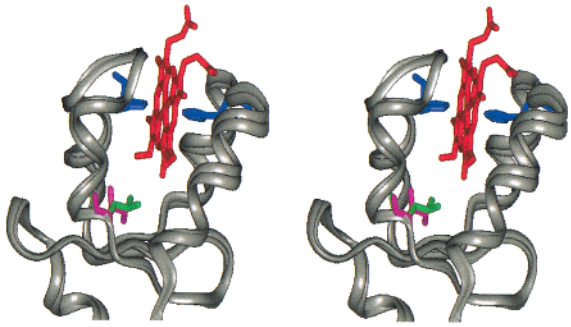

FIGURE 9: Stereoview highlighting differences in geometry of the side chains of Ile-32 (magenta) in wild-type rat OM cyt b_5 and Leu-32 (green) in the A18S/L47R/I32L triple mutant.

Position 71 in the mammalian Mc cytochromes b_5 is invariably occupied by Ser (see Figure 1), which has a small, polar side chain. In rat OM cyt b_5 residue 71 is a bulky, hydrophobic Leu. In the crystal structure of the rat OM cyt b_5 triple mutant, one of the δ-CH_3 groups of Leu-71 (light blue in Figure 8A) is positioned 3.7 Å from the same heme methyl group that is in contact with Leu-32 (B3Me). Hence, the larger size of Leu further restricts the space available to a heme substituent at this position. As a result, we predict that a vinyl group at this position (position 2 in isomer A; see Figure 7) will encounter energetically unfavorable steric interactions with the side chains of Leu-32 and Leu-71. These interactions should destabilize isomer A relative to isomer B in the triple mutant relative to the wild-type protein, a conclusion that is in good agreement with the A:B = 1:4 ratio measured by NMR spectroscopy. An identical steric microenvironment should exist in the I32L single mutant, consistent with the observation that it also exhibits an A:B ratio of 1:4.

In contrast, the X-ray crystal structure of wild-type rat OM cyt b_5 (Figure 8B) reveals that the side chain geometry of Ile-32 (blue) provides sufficient space at the bottom of the heme pocket to accommodate a methyl group (isomer B) or a vinyl group (isomer A), even in the presence of Leu-71 (light blue). These observations suggest that the stability of isomers A and B in wild-type rat OM cyt b_5 should be approximately the same, a conclusion that is also in good agreement with the 1:1.2 (A:B) ratio observed by NMR spectroscopy. The local environment in the A18S/L47R double mutant should be very similar, which is also consistent with the observation that the wild-type and double mutant proteins exhibit identical hemin isomer ratios.

The structures of wild-type rat OM cyt b_5 and of the A18S/L47R/I32L triple mutant, together with results obtained from ^{1}H NMR spectroscopic measurements, allowed us to conclude that heme−polypeptide interactions near residue 32 play a crucial role in stabilizing isomer B relative to isomer A in the single and triple mutants. It is therefore interesting to probe whether similar interactions are responsible for stabilizing isomer A relative to isomer B in the Mc cytochromes b_5. Inspection of the bovine Mc cyt b_5 structure (Figure 8C) revealed that the nature of residue 71 is likely to play a key role in stabilizing isomer A in Mc cytochromes b_5. As noted above, all mammalian Mc isoforms have Ser at position 71, whereas this position is occupied by Leu in

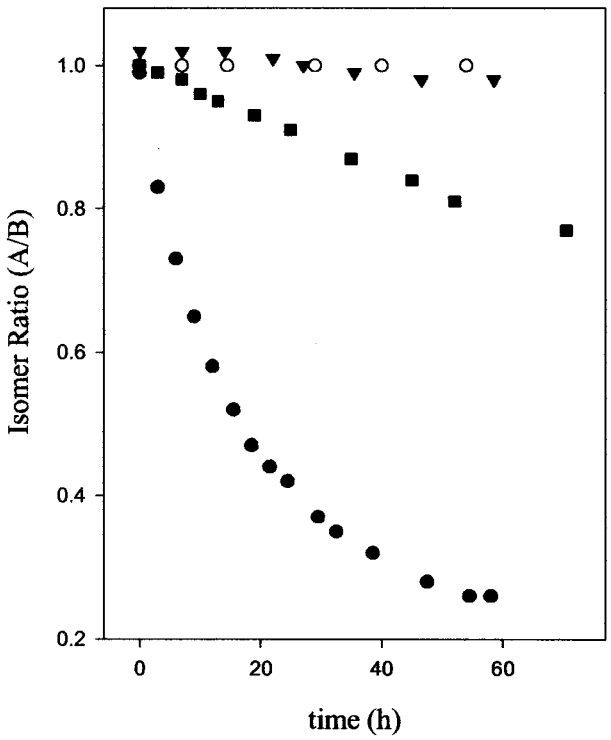

FIGURE 10: Time-dependent changes of the hemin isomer ratio obtained at 45 °C for wild-type rat OM cyt b_5 (○) A18S/L47R double mutant (▼), I32L mutant (■), and A18S/L47R/I32L triple mutant (●).

rat OM cyt b_5 (see Figure 1). It is evident from the structure of bovine Mc cyt b_5 (Figure 8C) that the side chain of Ser-71 (light blue) leaves ample room for accommodating a vinyl group (isomer A) at the bottom of the heme pocket, where it undergoes favorable hydrophobic interactions with Leu-32 (blue). In addition, the heme methyl group (A1Me) also interacts favorably with the methyl groups in the side chain of Leu-70 (magenta). However, if a vinyl group (isomer B) were to occupy this position, it is likely that unfavorable close contacts would develop between the vinyl group and the side chain of Leu-70. Consequently, it appears that an interplay between the spatial location of the side chains of Leu-70 and Ser-71 contributes to isomer A being thermodynamically favored in mammalian Mc cytochromes b_5.

Finally, we turned our attention to investigate whether the perturbation of the hydrophobic patch comprising residues Ala-18, Leu-32, Leu-36, and Arg-47 influenced the rate of hemin reorientation. To this end, we followed the time-dependent changes in the ^{1}H NMR spectra of wild-type rat OM cyt b_5 and of the three mutants prepared for this work, at pH = 7.0 and 45 °C. The results of these experiments, summarized in Figure 10, indicate that under the experimental conditions hemin in wild-type OM cyt b_5 and in the A18S/L47R double mutant is still kinetically trapped at physiologically relevant temperatures. We arrive at this conclusion based on the observation that, at 45 °C, the ratio of hemin orientational isomers (1:1) is time independent, despite the fact that the equilibrium constant K_{eq} = [B]/[A] observed for both proteins is 1.2 at 65 °C. In contrast, it is possible to observe the time-dependent conversion of isomer A into isomer B at pH 7.0 and 45 °C for the I32L and A18S/L47R/I32L mutants. It can be seen from Figure 10 that, in the case of the A18S/L47R/I32L triple mutant, the equilibrium ratio of orientational isomers ($K_{eq} = k_1/k_{-1} = 4$) is achieved in approximately 60 h. For the I32L single mutant, equilibration at 45 °C requires significantly longer incubation times.

When the data obtained for the triple mutant are analyzed in terms of the reversible first-order reaction described by eq 1 (see Experimental Procedures), a value of 0.05 h^{-1} is obtained for k_1. Consequently, isomer A in the A18S/L47R/I32L triple mutant exchanges into isomer B with a half-life of 13.5 h at pH 7.0 and 45 °C, whereas hemin in wild-type OM cyt b_5 is kinetically trapped under identical conditions. These findings suggest that the rates of hemin reorientation are related to the integrity of the hydrophobic patch that is unique to rat OM cyt b_5. When this patch in the mitochondrial protein is completely disrupted (i.e., in the triple mutant) hemin is no longer kinetically trapped at 45 °C. Nevertheless, the rate of hemin reorientation measured for the triple mutant at this temperature indicates that hemin reorientation is still significantly slower than that observed for bovine Mc cyt b_5, which exhibits a half-life of 13 h at 25 °C for the conversion of isomer B into isomer A (*32*). These observations, therefore, are in agreement with the trend observed using the various experimental measures of protein stability described herein to evaluate the effect of disrupting the hydrophobic microenvironment in rat OM cyt b_5. These findings indicated that although complete disruption of the hydrophobic microenvironment has been accomplished by preparing the A18S/L47R/I32L triple mutant, the properties of the latter have moved in the direction of, but are still different from, those of bovine Mc cyt b_5.

ACKNOWLEDGMENT

K.K. acknowledges the Center for Advanced Scientific Computing at the University of Kansas for use of the of SGI ORIGIN 2400 supercomputer, on which most of the simulations were performed. Funds for the Oklahoma Statewide Shared NMR facility were provided by the National Science Foundation (Grant BIR-952269), The Oklahoma State Regents for Higher Education, the W. M. Keck Foundation, and Conoco, Inc.

REFERENCES

1. Guzov, V. M., Houston, H. L., Murataliev, M. B., Walker, F. A., and Feyereisen, R. (1996) *J. Biol. Chem. 271*, 26637−26645.
2. Yu, Y., Yamasaki, H., Kita, K., and Shinzaburo, T. (1996) *Arch. Biochem. Biophys. 328*, 165−172.
3. Fukushima, K., and Sato, R. (1973) *J. Biochem. 74*, 161−173.
4. Ito, A. (1980) *J. Biochem. 87*, 63−71.
5. Lederer, F., Ghrir, R., Guiard, B., Cortial, S., and Ito, A. (1983) *Eur. J. Biochem. 132*, 95−102.
6. Mitoma, J., and Ito, A. (1992) *EMBO J. 11*, 4197−4203.
7. Borgese, N., D'Arrigo, A., De Silvestris, M., and Pietrini, G. (1993) *FEBS Lett. 325*, 70−75.
8. Kuroda, R., Ikenoue, T., Honsho, M., Tsujimoto, S., Mitoma, J., and Ito, A. (1998) *J. Biol. Chem. 273*, 31097−31102.
9. De Silvestris, M., D'Arrigo, A., and Borgese, N. (1995) *FEBS Lett. 370*, 69−74.
10. Ozols, J., and Heinemann, F. S. (1982) *Biochim. Biophys. Acta 704*, 163−173.
11. Ozols, J. (1989) *Biochim. Biophys. Acta 997*, 121−130.
12. Smith, M. A., Jonsson, L., Stymne, S., and Stobart, K. (1992) *Biochem. J. 287*, 141−144.

13. Deodutta, R., Strobel, H. W., and Liehr, J. G. (1991) *Arch. Biochem. Biophys. 285*, 331−338.
14. Kutay, U., Ahnert-Hilger, G., Hartmann, E., Wiedenmann, B., and Rapoport, T. A. (1995) *EMBO J. 14*, 217−233.
15. Vergères, G., Ramsden, J., and Waskell, L. (1995) *J. Biol. Chem. 270*, 3414−3422.
16. Kuroda, R., Kinoshita, J., Honsho, M., Mitoma, J., and Ito, A. (1996) *J. Biochem. 120*, 828−833.
17. Yoo, M., and Steggles, A. W. (1988) *Biochem. Biophys. Res. Commun. 156*, 576−580.
18. Cristiano, R. J., and Steggles, A. W. (1989) *Nucleic Acids Res. 17*, 799.
19. VanDerMark, P., and Steggles, A. W. (1997) *Biochem. Biophys. Res. Commun. 240*, 80−83.
20. Marra, M., Hillier, L., Allen, M., Bowles, M., Dietrich, N., Dubuquet, T., Geisel, S., Kucaba, T., Lacy, M., Le, M., Martin, J., Morris, M., Schellenberg, K., Steptoe, M., Tan, F., Underwood, K., Moore, B., Theising, B., Wylie, T., Lennon, G., Soares, B., Wilson, R., and Waterston, R. (1996) Direct Submission to the EMBL/GenBank/DDBJ Databases (accession code P56395).
21. Dariush, N., Fisher, C. W., and Steggles, A. W. (1988) *Protein Sequences Data Anal. 1*, 351−353.
22. Altschyl, S. F., Madden, T. L., Schäffer, A. A., Zhang, J., Zhang, Z., Miller, W., and Lipman, D. J. (1997) *Nucleic Acids Res. 25*, 3389−3402.
23. Rivera, M., Barillas-Mury, C., Christensen, K. A., Little, J. W., Wells, M. A., and Walker, F. A. (1992) *Biochemistry 31*, 12233−12240.
24. Mathews, F. S., Gerwinsky, E. W., and Argos, P. (1979) The X-ray Crystallographic Structure of Calf Liver Cytchrome b_5, in *The Porphyrins* (Dolphin, D., Ed.) pp 107−147, Academic Press, New York.
25. Silchenko, S., Sippel, M. L., Kuchment, O., Benson, D. R., Mauk, A. G., Altuve, A., and Rivera, M. (2000) *Biochem. Biophys. Res. Commun. 273*, 467−472.
26. Rodriguez-Maranon, M. J., Feng, Q., Stark, R. E., White, S. P., Zhang, X., Foundling, S. I., Rodriguez, V., Schilling, C. L., III, Bunce, R. A., and Rivera, M. (1996) *Biochemistry 35*, 16378−16390.
27. Durley, R. C. E., and Mathews, F. S. (1996) *Acta Crystallogr. D52*, 65−76.
28. Rivera, M., Wells, M. A., and Walker, F. A. (1994) *Biochemistry 33*, 2161−2170.
29. Rivera, M., Seetharaman, R., Ghirdhar, D., Wirtz, M., Zhang, X., Wang, X., and White, S. (1998) *Biochemistry 37*, 1485−1494.
30. Wirtz, M., Oganesyan, V., Zhang, X., Studer, J., and Rivera, M. (2000) *Faraday Discuss. 116*, 221−234.
31. Reid, L. S., Taniguchi, V. T., Gray, H. B., and Mauk, A. G. (1982) *J. Am. Chem. Soc. 104*, 7516−7519.
32. Walker, F. A., Emrick, D., Rivera, J. E., Hanquet, B. J., and Buttlaire, D. H. (1988) *J. Am. Chem. Soc. 110*, 6234−6240.
33. Mauk, A. G., Mauk, M. R., Moore, G. R., and Northrup, S. H. (1995) *J. Bioenerg. Biomembr. 27*, 311−330.
34. Rodgers, K. K., and Sligar, S. G. (1991) *J. Am. Chem. Soc. 113*, 9419−9421.
35. Ito, A., Hayashi, S., and Yoshida, T. (1981) *Biochem. Biophys. Res. Commun. 101*, 591−598.
36. Nishino, H., and Ito, A. (1986) *J. Biochem. 100*, 1523−1531.
37. Sawyer, D. T., Chiericato, G., and Tsuchiya, T. (1982) *J. Am. Chem. Soc. 104*, 6273−6278.
38. Storch, E. M., and Daggett, V. (1995) *Biochemistry 34*, 9682−9693.
39. Sambrook, J., Fritsch, E. F., and Maniatis, T. (1989) *Molecular Cloning: a Laboratory Manual*, 2nd ed., Cold Spring Harbor Laboratory, Cold Spring Harbor, NY.
40. Studier, F. W., and Moffatt, B. A. (1986) *J. Mol. Biol. 189*, 113−130.
41. La Mar, G. N., Toi, H., and Krishnamoorthi, R. (1984) *J. Am. Chem. Soc. 106*, 6395−6401.
42. Pace, C. N. (1986) *Methods Enzymol. 131*, 267−280.
43. Teale, F. W. J. (1959) *Biochim. Biophys. Acta 35*, 543.
44. Harrison, S. C., and Blout, E. R. (1964) *J. Biol. Chem. 240*, 299−303.
45. Bauer, G., and Silfen, J. (1982) *Biopolymers 21*, 2399−2411.
46. Otwinowski, Z., and Minor, W. (1997) *Methods Enzymol. 276*, 307−326.
47. Navaza, J. (1994) *Acta Crystallogr. A50*, 157−163.
48. Brunger, A. T., Kuriyan, J., and Karplus, M. (1987) *Science 235*, 458−460.
49. Roussel, A., and Cambillau, C. (1989) *Silicon Graphics Geometry Partners Directory*, Silicon Graphics, Mountain View, CA.
50. Jones, T. A., and Zhou, J. Y. (1991) *Acta Crystallogr A47*, 110−119.
51. Laskowski, R. A., MacArthur, M. W., Moss, D. S., and Thornton, J. M. (1993) *J. Appl. Crystallogr. 26*, 477−486.
52. Brooks, B. R., Buccoleri, R., Olafson, B., States, S., Swaminathan, S., and Karplus, M. (1983) *J. Comput. Chem. 4*, 187−217.
53. MacKerell, A. D., Jr., Bashford, D., Bellott, M., Dunbrack, R. L., Jr., Evanseck, J. D., Field, M. J., Fischer, S., Gao, J., Guo, H., Ha, S., Michnick, S., Ngo, T., Nguyen, D. T., Prodhom, B., Reiher, W. E., III, Roux, B., Schlenkrich, M., Smith, J. C., Stote, R., Straub, J., Watanabe, M., Wiorkewicz-Kuczera, J., Yin, D., and Karplus, J. (1998) *J. Phys. Chem. B 102*, 3586−3616.
54. Brunger, A. T., and Karplus, M. (1988) *Proteins 4*, 148−156.
55. Grubmueller, H. (1994) Ph.D. Dissertation, Ludwig-Maximilians University, Muenchen.
56. Leach, A. R. (1996) *Molecular Modeling. Principles and Applications*, Longman, Harlow, U.K.
57. Allen, M. P., and Tildesley, D. J. (1987) *Computer-Simulations of Liquids*, Oxford Science Publications, London.
58. Ryckaert, J. P., Ciccotti, G., and Berendsen, H. J. C. (1977) *J. Comput. Phys. 23*, 327−341.
59. Feller, S. E., Zhang, Y., and Pastor, R. W. (1995) *J. Chem. Phys. 103*, 4613−4621.
60. Sangui, C., and Darden, T. A. (1999) *Annu. Rev. Biophys. Biomol. Struct. 28*, 155−179.
61. Moore, C. D., and Lecomte, J. T. J. (1993) *Biochemistry 32*, 199−207.
62. Storch, E. M., and Daggett, V. (1996) *Biochemistry 35*, 11596−11604.
63. Storch, E. M., Daggett, V., and Atkins, W. M. (1999) *Biochemistry 38*, 5054−5064.
64. Smith, M. L., Olson, J., Hjortsberg, K., and Paul, K. G. (1991)- *Proc. Natl. Acad. Sci. U.S.A. 88*, 882−886.
65. Hargrove, M. S., Singleton, E. W., Quillin, M. L., Ortiz, L. A., Phillips, G. N. J., Mathews, A. J., and Olson, J. S. (1994) *J. Biol. Chem. 269*, 4207−4214.
66. Rivera, M., Qiu, F., Bunce, R. A., and Stark, R. E. (1999) *J. Biol. Inorg. Chem. 4*, 87−98.
67. La Mar, G. N. (1978) *Proc. Natl. Acad. Sci. U.S.A. 75*, 5755−5759.
68. La Mar, G. N., Burns, P. D., Jackson, J. T., Smith, K. M., Langry, K. C., and Strittmatter, P. (1981) *J. Biol. Chem. 256*, 6075−6079.
69. McLachlan, S. J., La Mar, G. N., Burns, P. D., Smith, K. M., and Langry, K. C. (1986) *Biochim. Biophys. Acta 874*, 274−284.
70. McLachlan, S. J., La Mar, G. N., and Sletten, E. (1986) *J. Am. Chem. Soc. 108*, 1285−1291.
71. Mortuza, G. B., and Whitford, D. (1997) *FEBS Lett. 412*, 610.
72. Hewson, R., Newbold, R. J., and Whitford, D. (1993) *Protein Eng. 6*, 953.
73. Manyusa, S., and Whitford, D. (1999) *Biochemistry 38*, 9333−9340.

BI010636I